Research Inventy: International Journal of Engineering and Science
Vol.16, Issue 5 (May 2026), PP 41-50
Issn (e): 2278-4721, Issn (p):2319-6483, www.researchinventy.com

Optimization of Offshore Wind Turbine Blades Using the EDAS Method

Minh Huy Nguyen*, Tan Ken Nguyen

Faculty of Mechanical engineering and Technology, Ho Chi Minh City University of Industry and Trade, 140 Le Trong Tan, Tay Thanh, Ho Chi Minh City, Vietnam, 700000

Abstract: *This study focuses on optimizing the design of wind turbine blades by investigating geometric parameters (tilt angle, blade thickness) and manufacturing materials. By combining the Taguchi method to establish 27 experimental models and performing aerodynamic simulations using Inventor software, characteristics such as airflow velocity and mechanical strength were analyzed at different input velocities (50–60 m/s). To select the most optimal variant, the study employed the Entropy method to determine criteria weights and the EDAS (Evaluation based on Distance from Average Solution) method to rank the configurations. The results identified the optimal model as having a thickness of 640 mm, a tilt angle of 12°, an input velocity of 55 m/s, and being made of aluminum alloy. This configuration balances aerodynamic efficiency (blade velocity of 107 m/s) and durability (stress of 31.228 MPa), while reducing weight by 5% compared to previous designs.*

Keywords: *Wind turbine blade, EDAS method, Entropy weight, Multi-objective optimization, Aerodynamic performance.*

Date of Submission: 05-05-2026 Date of Acceptance: 15-05-2026

I. INTRODUCTION

The global transition toward sustainable energy has placed wind power at the forefront of technological innovation, necessitating continuous improvements in the efficiency, structural integrity, and environmental sustainability of turbine systems. As wind turbines increase in scale and are deployed in more challenging environments, the industry faces complex hurdles ranging from aerodynamic degradation to structural fatigue and end-of-life waste management. To address these challenges, recent international research has focused on integrating high-fidelity simulations with advanced optimization and diagnostic frameworks. The advancement of aerodynamic performance remains a primary research frontier. Under harsh operating conditions where surface roughness typically degrades power output, the application of vortex generators has been proven to delay flow separation, increasing the power coefficient by up to 47.8% [1]. Such aerodynamic refinements are increasingly being coupled with sophisticated structural optimization. For instance, the use of conjugate gradient methods and non-linear fatigue analysis allows for the optimization of complex blade root architectures involving thousands of design variables, achieving substantial mass reduction without compromising safety [2]. Furthermore, multidisciplinary design optimization (MDO) frameworks now utilize Kriging models and genetic algorithms to synchronize aerodynamic shapes with finite element structural verification, ensuring optimal chord length, twist angles, and shell thickness [3]. Beyond design and simulation, the industry is embracing digital transformation and intelligent diagnostics to enhance operational reliability. The integration of improved deep learning models, such as DCW-YOLO based on YOLOv8, has enabled the high-precision detection of surface damage via UAV imagery, achieving mAP scores as high as 93.8% [4]. At the system level, reinforcement learning-based particle swarm optimization (RPSO) is being deployed to solve complex wind farm layout problems (WFLO), effectively mitigating wake effects and reaching power conversion efficiencies of 98.68% [5]. To complement these digital strides, non-contact structural health monitoring using Laser Doppler Vibrometers (LDV) and Hilbert-Huang transforms provides a reliable, non-invasive method for detecting internal cracks in composite blades [6]. The diversification of turbine architectures and sustainable lifecycles also represents a critical research direction. Investigations into double-rotor Darrieus vertical axis wind turbines (DD-VAWT) have identified blade chord length as a dominant factor in performance optimization [7]. Simultaneously, the environmental impact of decommissioned blades is being addressed through circular economy initiatives, such as recycling blade waste into concrete additives to improve mechanical strength and reduce carbon emissions [8]. Automated design methods for airfoils continue to push the limits of lift-to-drag ratios, achieving torque coefficient improvements of 5.5% in small-scale systems [9]. Furthermore, the shift toward natural fibers like flax and basalt is projected to

reduce Global Warming Potential (GWP) by up to 8% compared to traditional glass fibers [10]. Finally, the development of passive-controlled flexible blades made from GFRP composites offers promising solutions for small-scale wind energy conversion systems (WECS), ensuring stable power output and effective self-starting capabilities [11]. Collectively, these advancements provide a robust scientific framework for the next generation of resilient and high-performance wind energy infrastructure.

II. OPTIMIZATION METHOD

2.1 Determination of Objective Weights by the Entropy Technique

The Entropy method is a quantitative approach for determining the objective weights of criteria in Multi-Criteria Decision-Making (MCDM) problems. This method is rooted in Information Entropy theory, which measures the degree of uncertainty (entropy) associated with each specific criterion

Steps of the Entropy Weight Method for Weight Calculation [12-16]

Data Normalization Process

The obtained experimental or simulation data must be normalized using the following equation:

Maximization criteria:

$$r_{ij} = \frac{x_{ij} - \min(x_j)}{\max(x_j) - \min(x_j)} \tag{1}$$

Minimization criteria

$$r_{ij} = \frac{\max(x_j) - x_{ij}}{\max(x_j) - \min(x_j)} \tag{2}$$

$$\omega_e(x) = x.e^{(1-x)} + (1-x)e^x - 1 \tag{3}$$

Where $\omega_e(x)$ represent the mapping function in the entropy measurement. The function reaches its maximum value at x=0.5, and $e^{0.5} - 1$=0.6487, the mapped values within the range [0,1] are determined as follows:

$$w \equiv \frac{1}{(e^{0.5} - 1)} \sum_{i=1}^{m} \omega_e(x) \tag{4}$$

Determine the Normalization Coefficient

$$k = \frac{1}{(e^{0.5} - 1) \times m} = \frac{1}{0.6487 \times m} \tag{5}$$

determine entropy

$$e_j = k \sum_{i=1}^{m} \omega_e \left(\frac{\gamma_i(j)}{D_j}\right), j = 1,2,...,n \tag{6}$$

where, $\omega_e(x)$ Applying the formula (6)

Calculate the summation entropy using the formula (7)

$$E = \sum_{j=1}^{n} e_j \tag{7}$$

Determine the weighting factors

$$W_j = \frac{1}{n-E} \cdot \frac{[1-e_j]}{\sum_{j=1}^{n} \frac{1}{n-E} \cdot [1-e_j]}, \; j = 1,2,...,n. \tag{8}$$

2.2 The optimal turbine blade model using the EDAS method

The Evaluation based on Distance from Average Solution (EDAS) is a robust multi-criteria decision-making (MCDM) framework. Given the requirement for the proposed model to achieve high amplification performance while maintaining low stress levels, the task is defined as a multi-objective optimization problem. Consequently,

the implementation of the EDAS method is imperative to validate the optimal configuration of the design variables. The systematic execution of the EDAS algorithm [17-19] for multi-criteria decision-making involves the following steps

- *Step 1: Constructing the decision matrix, which integrates all evaluation criteria and objectives into a structured matrix format*

$$X = [x_{ij}]_{m\times n} = \begin{bmatrix} x_{11} & \cdots & x_{1n} \\ x_{21} & \cdots & x_{1n} \\ \vdots & \cdots & x_{2n} \\ x_{m1} & \cdots & x_{mn} \end{bmatrix} \tag{9}$$

m representing the number of experimental trials or numerical simulations, n denoting the number of criteria or objective functions, x_{ij} denoting the number of criteria or objective functions i.

- *Step* 2: The Average Solution (AVG) for all alternatives is determined as follows:

$$AVG = \frac{\sum_{i=1}^{m} x_i}{m} \tag{10}$$

- *step 3: Calculation of the Positive Distance from Average (PDA) and the Negative Distance from Average (NDA):*

$$PD_{ij} = \frac{\max[0,(x_{ij} - AVG_j)]}{AVG_j} \tag{11}$$

$$PD_{ij} = \frac{\max[0,(AVG_j - x_{ij})]}{AVG_j} \tag{12}$$

$$ND_{ij} = \frac{\max[0,(AVG_j - x_{ij})]}{AVG_j} \tag{13}$$

$$ND_{ij} = \frac{\max[0,(x_{ij} - AVG_j)]}{AVG_j} \tag{14}$$

- *Step 4: Determination of the Weighted Sum of Positive Distances (SoP) and the Weighted Sum of Negative Distances (SoN).*

$$SoP_i = \sum_{i=1}^{m} w_j . PD_{ij} \tag{15}$$

$$SoN_i = \sum_{i=1}^{m} w_j . ND_{ij} \tag{16}$$

W_j denoting the weight of the criterion j.

- *Step 5: The SSoP and SSoN values are normalized using the following formulas:*

$$SSoP_i = \frac{SoP_i}{\max(SoP_i)} \tag{17}$$

$$SSoN_i = \frac{SoN_i}{\max(SoN_i)} \tag{18}$$

- *Step 6: The Appraisal Score APS_i for each alternative is calculated using the following formula*

$$APS_i = \frac{1}{2}(SSoP_i + SSoN_i) \tag{19}$$

- *Step 7: The alternatives are ranked in descending order, where the candidate with the highest APS_i value represents the optimal solution*

III. DESIGN AND ANALYTICAL METHODOLOGY FOR WIND TURBINE BLADE MODELING

3.1 Geometric Modeling

The offshore wind turbine substructure was modeled using Autodesk Inventor, generating 27 distinct geometric configurations for parametric analysis and selection. A Finite Element Analysis (FEA) workflow was established, utilizing ANSYS CFD to compute the aerodynamic pressure fields, which were subsequently mapped onto a Static Structural environment to evaluate the velocity distributions and structural stress profiles of the turbine blades. This comprehensive dataset of 27 simulation cases served as the basis for multi-criteria optimization. Specifically, the Taguchi method and FEA results were integrated with the EDAS (Evaluation based on Distance from Average Solution) to identify the optimal design among the candidates.

The offshore wind turbine blade in this study was engineered within the Inventor environment, as illustrated in Figure 2.1. Figure 2.2 provides the orthographic projections of the offshore wind turbine assembly. The designed rotor radius is 59 m. The blade tilt angle, measured relative to the horizontal plane, was varied across three levels: 12°, 14°, and 16°. The blade thickness was evaluated at 650 mm, 640 mm, and 630 mm. For the material selection phase, three high-performance alloys Aluminum alloy, Magnesium alloy, and Titanium alloy—were incorporated into the simulation matrix

Figure 1. Geometric design of the offshore wind turbine blade.

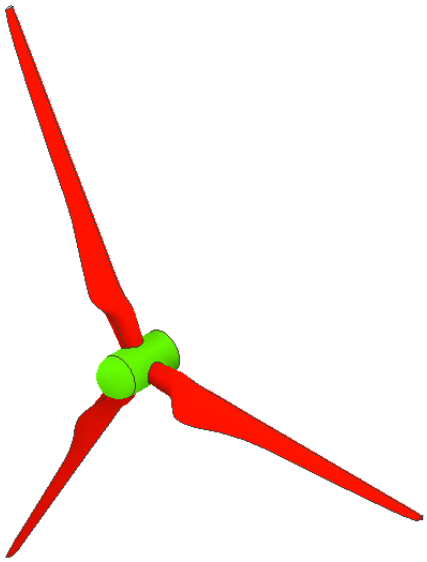

Figure 2. Orthographic projections of the offshore wind turbine blade

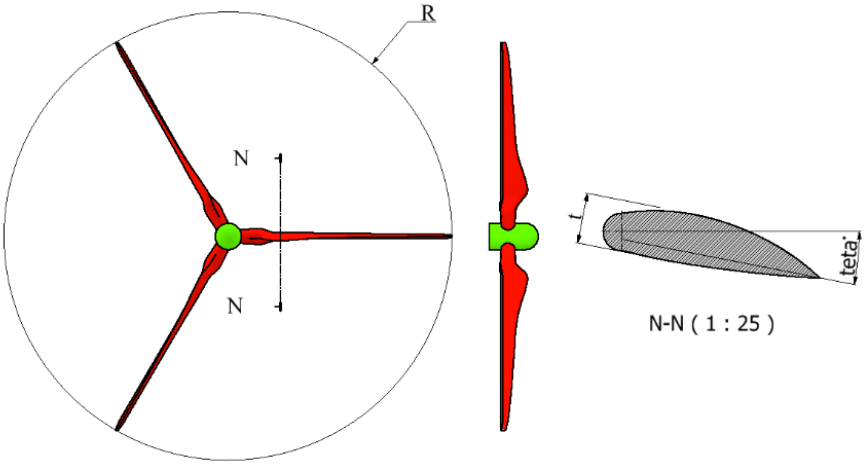

3.2. Aerodynamic modeling of loads acting on offshore wind turbine blades

Table 1. Implementation of Boolean operations for domain initialization and obstacle generation.

Details of Boolean1	
Boolean	Boolean1
Operation	Subtract
Target Bodies	2 Bodies
Tool Bodies	1 Body
Tool Bodies?	No

Figure 3. Computational domain initialization resulting from Boolean operations.

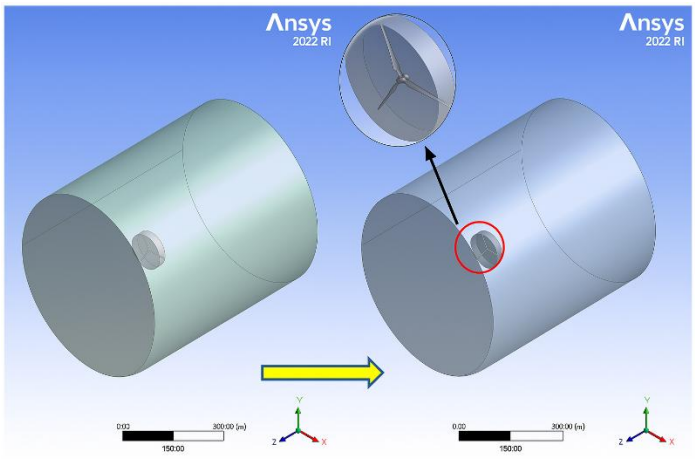

The fluid domain, established after the Boolean subtract operation as illustrated in Figure 3, facilitates a clear distinction between the fluid flow channels and the structural boundaries. This extracted volume constitutes the final computational domain. This step is critical for ensuring high-fidelity mesh generation and the accurate definition of boundary conditions throughout the numerical simulation process.

Figure 4. Mesh generation results

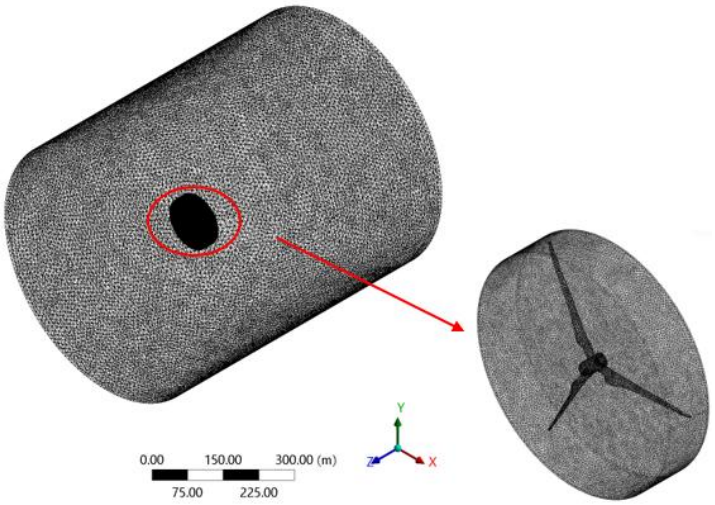

The detailed integration of the rotor mesh within the global computational domain is illustrated in Figure 4. The left portion of the figure highlights the refined mesh region surrounding the rotor, demarcated by a red ellipse, to emphasize the high-resolution elements required to capture complex flow interactions. The right portion provides a magnified view of the meshed three-blade rotor, clearly depicting the dense mesh distribution along the blade surfaces.

This integrated meshing strategy ensures precise coupling between the rotating blades and the surrounding fluid, which is fundamental for accurately capturing the aerodynamic performance of the offshore wind turbine system.

The global computational domain was discretized with a mesh size of 0.7 m. This resulted in a total of 1,890,732 triangular elements and 2,612,046 nodes. For the turbine blades, an automated meshing approach was employed, yielding a local mesh density of 50,234 triangular elements and 89,737 nodes.

Minitab software was employed to develop an experimental design comprising 27 runs. The design parameters were defined as follows: the inlet wind velocity was set at three levels: 50 m/s, 55 m/s, and 60 m/s. The materials investigated in this study included three distinct alloys: aluminum, titanium, and magnesium, represented by their respective Poisson's ratios of 0.33, 0.34, and 0.35. Furthermore, the turbine blade thickness was simulated at three levels: 630 mm, 640 mm, and 650 mm, while the blade pitch angles were established at 12°, 14°, and 16°. All design parameter values are systematically documented in Table 2

Table 2. Design parameters and corresponding levels

Parameter	Symbol	Unit	Level 1	Level 2	Level 3
Inlet wind velocity	v	m/s	50 m/s	55 m/s	60 m/s
Index poisson	p		0.33	0.34	0.35
Turbine blade thickness	t	mm	650	640	630
Pitch angle	Teta	angle	12	14	16

Figure 5. Applied boundary conditions and loads

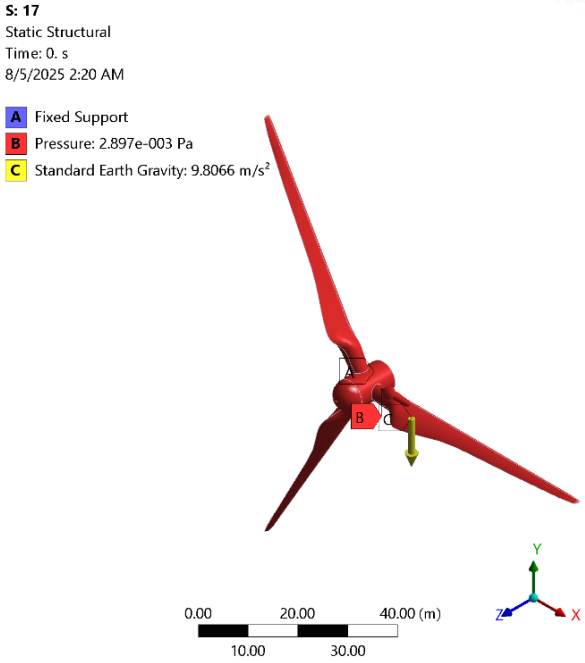

To evaluate the structural response of the wind turbine blade, a static structural analysis was performed using ANSYS. The Fixed Support boundary condition was applied to the blade root, effectively constraining all six degrees of freedom to simulate the rigid connection between the blade and the turbine hub. The loading conditions consist of both aerodynamic and body forces. The external wind load was modeled as a constant Wind Pressure of 0.002897 Pa, acting normally to the blade's suction and pressure surfaces to represent the aerodynamic lift and drag. Furthermore, Standard Earth Gravity of 9.81 m/s^2 was integrated into the model to account for the gravitational effects and the self-weight of the composite structure. This comprehensive setup ensures an accurate assessment of the equivalent stress distributions and total deformation across the blade geometry under operating conditions as presented in Figure 5.

IV. RESULTS AND DISCUSSION

4.1 Results of Entropy Method

The results of weight determination using the Entropy Weight Method (EWM) are summarized in Table 3. In this table:

- *The first column represents the model cases.*
- *The second and third columns are obtained by normalizing the data derived from Computational Fluid Dynamics (CFD) and Structural Analysis. Specifically, the wind velocity across the turbine blades and the blade stress were normalized by substituting their respective values into Equations (1) and (2).*
- *The mapping values and the mapping function results, determined via Equations (3), are recorded in the fourth and fifth columns.*
- *The efficiency after eliminating individual criteria is determined by Equation (4) and recorded in columns 6 and 7.*
- *Finally, the weighting factors for velocity and stress were found to be 0.5001 and 0.4999, respectively, as calculated by Equation (6).*

Table 3. Weighting factors calculated by Entropy technique

Model	nij		wev	wes	we*(rj/dj)	we*(rj/dj)
1	0.0620	0.6492	0.1564	0.5934	0.0039	0.0239
2	0.1983	0.5735	0.4196	0.6353	0.0115	0.0235
3	0.1033	0.5864	0.2475	0.6302	0.0063	0.0236
4	0.1653	0.5605	0.3656	0.6397	0.0098	0.0233
5	0.3182	0.5363	0.5665	0.6455	0.0171	0.0229
6	0.2901	0.5605	0.5388	0.6397	0.0159	0.0233
7	0.2562	0.6596	0.5000	0.5854	0.0143	0.0238
8	0.3595	0.6200	0.5997	0.6130	0.0187	0.0238
9	0.1322	0.6241	0.3053	0.6105	0.0080	0.0238
10	0.3926	0.6697	0.6201	0.5771	0.0199	0.0238
11	0.2273	0.5710	0.4621	0.6362	0.0129	0.0234
12	0.4339	0.5755	0.6379	0.6346	0.0213	0.0235
13	0.1942	0.6353	0.4132	0.6033	0.0113	0.0239
14	0.1488	0.5395	0.3363	0.6449	0.0089	0.0230
15	0.3595	0.9493	0.5997	0.1297	0.0187	0.0081
16	0.0000	0.8765	0.0000	0.2884	0.0000	0.0158
17	0.4380	1.0000	0.6392	0.0000	0.0214	0.0000
18	0.4711	0.9672	0.6264	0.0885	0.0204	0.0057
19	0.7066	0.1293	0.5423	0.2997	0.0243	0.0075
20	0.7521	0.2204	0.4896	0.4524	0.0233	0.0121
21	0.7893	0.0769	0.4384	0.1905	0.0220	0.0046
22	0.7975	0.0628	0.4261	0.1583	0.0216	0.0038
23	0.8554	0.1368	0.3286	0.3141	0.0182	0.0079
24	0.8802	0.0000	0.2811	0.0000	0.0162	0.0000
25	1.0000	0.0216	0.0000	0.0572	0.0000	0.0013
26	0.9380	0.1263	0.1564	0.2939	0.0099	0.0073
27	0.6364	0.0418	0.6025	0.1081	0.0249	0.0025

The subsequent results of the Entropy Weight Method are presented in Table 4. The entropy values were determined using Equation (6) and are recorded in columns 1 and 2. The total entropy was calculated via Equation (7) and is documented in column 3. Furthermore, the weighting factors were derived from Equation (8) and are

reported in columns 6 and 7. Consistent with the previous analysis, the weights for velocity and stress were found to be 0.5001 and 0.4999, respectively.

Table 4. Entropy values and weighting factors

e1	e2	E	(1/(m-E)*(1-e1)	(1/(m-E)*(1-e2)	W1	W2
0.0229	0.0232	0.0460	0.5001	0.4999	0.5001	0.4999

4.2 EDAS results with weights derived from Entropy technique

Similarly, by employing the weighting factors derived from the Entropy technique, the Average Solution, as well as the Positive and Negative Distances for the two criteria—velocity across the turbine blade and blade stress were determined. These values were calculated using Equations (12) to (14) and are documented in Table 5.

Table 5. Positive and negative distances from the average solution.

Model	PDij		NDij	
	V	St	V	St
1	0.00000	0.13933	0.11635	0.00000
2	0.00000	0.07688	0.07421	0.00000
3	0.00000	0.08751	0.10358	0.00000
4	0.00000	0.06619	0.08443	0.00000
5	0.00000	0.04617	0.03718	0.00000
6	0.00000	0.06619	0.04587	0.00000
7	0.00000	0.14797	0.05634	0.00000
8	0.00000	0.11527	0.02441	0.00000
9	0.00000	0.11867	0.09465	0.00000
10	0.00000	0.15631	0.01420	0.00000
11	0.00000	0.07481	0.06528	0.00000
12	0.00000	0.07857	0.00143	0.00000
13	0.00000	0.12787	0.07549	0.00000
14	0.00000	0.04881	0.08954	0.00000
15	0.00000	0.38700	0.02441	0.00000
16	0.00000	0.32692	0.13551	0.00000
17	0.00000	0.42888	0.00015	0.00000
18	0.00000	0.40092	0.01037	0.00000
19	0.08285	0.00000	0.00000	0.28971
20	0.09690	0.00000	0.00000	0.21454
21	0.10839	0.00000	0.00000	0.33290
22	0.11094	0.00000	0.00000	0.34457
23	0.12882	0.00000	0.00000	0.28349
24	0.13648	0.00000	0.00000	0.39640
25	0.17351	0.00000	0.00000	0.37861
26	0.15436	0.00000	0.00000	0.29212
27	0.06114	0.00000	0.00000	0.36194

The results of the EDAS method are documented in Table 5. Specifically, the Weighted Sum of Positive Distances (SoPi), determined by Equation (15), is recorded in the second column, while the Weighted Sum of Negative Distances (SoNi), calculated via Equation (16), is presented in the third column. Subsequently, the normalized weighted values derived from Equations (17) and (18) are logged in the fourth and fifth columns, respectively. The final Appraisal Scores , calculated using Equation (19), are listed in the sixth column, followed by the final ranking. The highest APSi value is assigned Rank 1, with subsequent values ranked down to Rank 27. Case 17th achieved the first rank, signifying the optimal configuration. The results identify the optimal turbine blade model as follows: aluminum alloy material, 640 mm thickness, and a 12° tilt angle. Under these conditions, the airflow velocity across the blade reaches 107 m/s, while the induced stress is 31.228 MPa a relatively high velocity paired with a stress level significantly below the material's ultimate strength. Furthermore, the blade's weight was reduced from an initial 3 tons to 2.25 tons, representing a 25% total mass reduction after optimization.

Table 5. Weighted sums, normalized values, appraisal scores, and final ranking of the alternatives

Model	SoPi	SoNi	SSoPi	SSoNi	APSi	rank
1	0.06965	0.05819	0.32488	0.70635	0.51562	12
2	0.03843	0.03711	0.17925	0.81270	0.49598	15
3	0.04374	0.05180	0.20403	0.73858	0.47131	16
4	0.03309	0.04222	0.15433	0.78692	0.47063	17
5	0.02308	0.01860	0.10765	0.90616	0.50690	13
6	0.03309	0.02294	0.15433	0.88425	0.51929	10
7	0.07397	0.02817	0.34502	0.85782	0.60142	7
8	0.05762	0.01221	0.26877	0.93839	0.60358	6
9	0.05932	0.04733	0.27670	0.76114	0.51892	11
10	0.07814	0.00710	0.36447	0.96417	0.66432	5
11	0.03740	0.03264	0.17442	0.83526	0.50484	14
12	0.03928	0.00071	0.18320	0.99640	0.58980	8
13	0.06392	0.03775	0.29815	0.80948	0.55381	9
14	0.02440	0.04478	0.11381	0.77403	0.44392	18
15	0.19346	0.01221	0.90237	0.93839	0.92038	3
16	0.16343	0.06777	0.76228	0.65801	0.71015	4
17	0.21440	0.00008	1.00000	0.99962	0.99981	1
18	0.20042	0.00518	0.93482	0.97384	0.95433	2
19	0.04143	0.14483	0.19326	0.26914	0.23120	22
20	0.04846	0.10725	0.22602	0.45876	0.34239	19
21	0.05421	0.16642	0.25283	0.16019	0.20651	24
22	0.05548	0.17225	0.25879	0.13075	0.19477	25
23	0.06442	0.14171	0.30049	0.28484	0.29266	21
24	0.06825	0.19816	0.31836	0.00000	0.15918	26
25	0.08677	0.18927	0.40474	0.04487	0.22480	23
26	0.07719	0.14603	0.36006	0.26305	0.31155	20
27	0.03058	0.18093	0.14262	0.08693	0.11477	27

The optimization results indicate a maximum airflow velocity of 107 m/s across the turbine blade. This high-velocity flow induces a total deformation of 82.464 mm and an equivalent stress of 31.228 MPa. Despite the significant deformation, the relatively low stress levels ensure that the turbine blade maintains sufficient structural integrity and durability under extreme storm conditions

V. CONCLUSIONS

Based on the comprehensive analysis and optimization results, this research draws the following key conclusions:

- Influence of Parameters: The inlet airflow velocity and the blade tilt angle are the two most decisive factors affecting aerodynamic characteristics and mechanical stress. In contrast, blade thickness and the material's Poisson's ratio exhibit a lower degree of influence.
- Efficiency of EDAS and Entropy Methods: The application of the Entropy weight method effectively eliminated subjectivity in weight assignment. Combined with the EDAS algorithm, it accurately identified the optimal configuration. The deviation between the actual simulation and the predicted results remained exceptionally low (under 2.5%), confirming the high reliability of the computational framework.
- Optimal Parameters: The ideal configuration was determined to be a 12° tilt angle utilizing aluminum alloy. Under these conditions, the turbine blade not only maximizes power generation performance but also achieves structural optimization, resulting in a 5% reduction in total mass.
- Practical Value: The integrated research framework—combining the Taguchi method, numerical simulation, and Multi-Criteria Decision-Making (MCDM)—represents a highly effective approach. This methodology significantly shortens the design cycle and reduces manufacturing costs, contributing to the sustainable development of the wind energy industry.

Conflict of interest

There is no conflict to disclose.

ACKNOWLEDGEMENT

The author would like to express their sincere gratitude to Ho Chi Minh City University of Industry and Trade (HUIT) for providing a supportive academic environment and the necessary resources to complete this research

REFERENCES

[1] Y. Yang et al., 2025. Enhancing Aerodynamic Performance of Horizontal Axis Wind Turbine Blade Aerodynamic Performance Under Rough Wall Condition Using Vortex Generators. *Journal of Marine Science and Engineering* 13, 397-415, doi: 10.3390/jmse13030397.
[2] S. M. Hermansen, T. Macquart, and E. Lund, 2025. Gradient-based structural optimization of a wind turbine blade root section including high-cycle fatigue constraints. *Engineering Optimization* 57, 1-32, doi: 10.1080/0305215x.2024.2428678.
[3] F. He et al., 2025. Collaborative Optimization of Aerodynamics and Wind Turbine Blades. *Applied Sciences* 15, 834, doi: 10.3390/app15020834.
[4] L. Zou, A. Chen, C. Li, X. Yang, and Y. Sun, 2024. DCW-YOLO: An Improved Method for Surface Damage Detection of Wind Turbine Blades. *Applied Sciences* 14, 8763, doi: 10.3390/app14198763.
[5] Z. Zhang, J. Li, Z. Lei, Q. Zhu, J. Cheng, and S. Gao, 2024. Reinforcement learning-based particle swarm optimization for wind farm layout problems. *Energy* 313, 134050, doi: 10.1016/j.energy.2024.134050.
[6] A. Zabihi et al., 2024. Non-Contact Wind Turbine Blade Crack Detection Using Laser Doppler Vibrometers. *Energies* 17, 2165, doi: 10.3390/en17092165.
[7] Z. Shen, S. Gong, G. Xie, H. Lu, and W. Guo, 2024. Investigation of the effect of critical structural parameters on the aerodynamic performance of the double darrieus vertical axis wind turbine. *Energy* 290, 130156, doi: 10.1016/j.energy.2023.130156.
[8] V. Revilla-Cuesta, J. Manso-Morato, N. Hurtado-Alonso, M. Skaf, and V. Ortega-López, 2024. Mechanical and environmental advantages of the revaluation of raw-crushed wind-turbine blades as a concrete component. *Journal of Building Engineering* 82, 108383, doi: 10.1016/j.jobe.2023.108383.
[9] J. Radi, J. E. Sierra-García, M. Santos, C. Armenta-Déu, and A. Djebli, 2024. Metaheuristic Optimization of Wind Turbine Airfoils with Maximum-Thickness and Angle-of-Attack Constraints. *Energies* 17, 6440, doi: 10.3390/en17246440.
[10] K. Pender, K. Bacharoudis, F. Romoli, P. Greaves, and J. Fuller, 2024. Feasibility of Natural Fibre Usage for Wind Turbine Blade Components: A Structural and Environmental Assessment. *Sustainability* 16, 5533, doi: 10.3390/su16135533.
[11] N. Papadakis and C. Condaxakis, 2024. An Experimental Performance Assessment of a Passively Controlled Wind Turbine Blade Concept: Part B—Material Oriented with Glass-Fiber-Reinforced Polymer. *Energies* 17, 3286, doi: 10.3390/en17133286.
[12] K. Vasantha Lakshmi and K. N. Udaya Kumara, 2025. Fuzzy MCDM techniques for portfolio selection in the post-COVID Indian mutual fund market: a comparative study of FAHP and entropy methods. *Journal of Ambient Intelligence and Humanized Computing* 16, 97-107, doi: 10.1007/s12652-024-04886-9.
[13] Y. Wang, Y. Li, H. Li, W. Dang, and A. Zheng, 2025. Study on the correlation between soil resistivity and multiple influencing factors using the entropy weight method and genetic algorithm. *Electric Power Systems Research* 246, 111692, doi: 10.1016/j.epsr.2025.111692.
[14] H. Huang et al., 2025. Comprehensive evaluation of peptides quality using a “quantity-activity integration” approach with a portable NIR spectrometer and entropy weighted TOPSIS method. *Microchemical Journal* 213, 113673, doi: 10.1016/j.microc.2025.113673.
[15] L. Jing, L. Ke, Z. Lei, Y. Xiaoya, J. Yuanyuan, and J. Huinan, 2024. Geohash coding location privacy protection scheme based on entropy weight TOPSIS. *The Journal of Supercomputing* 81, 85, doi: 10.1007/s11227-024-06511-0.
[16] S. G. Ghalme, I. Momohjimoh, Y. Falak, and R. K. Thakur, 2025. Investigation of Mechanical Properties of Groundnut-Based Composite Using the Entropy-Weighted TOPSIS Approach. *International Journal of Automotive and Mechanical Engineering* 22, 12062-12073, doi: 10.15282/ijame.22.1.2025.9.0926.
[17] G. Wei, C. Wei, and Y. Guo, 2021. EDAS method for probabilistic linguistic multiple attribute group decision making and their application to green supplier selection. *Soft Computing* 25, 9045-9053, doi: 10.1007/s00500-021-05842-x.
[18] C. Wei, J. Wu, R. Wang, G. Wei, F. Lei, and Y. He, 2019. EDAS Method for Multiple Attribute Group Decision Making with Probabilistic Uncertain Linguistic Information and Its Application to Green Supplier Selection. *International Journal of Computational Intelligence Systems* 12, 1144-1154, doi: 10.2991/ijcis.d.191028.001.
[19] D. Peng, J. Wang, D. Liu, and Z. Liu, 2022. An Improved EDAS Method for the Multi-Attribute Decision Making Based on the Dynamic Expectation Level of Decision Makers. *Symmetry* 14, 979, doi: 10.3390/sym14050979.